NUMERICAL INVESTIGATION OF NONLINEAR HEAT TRANSFER EFFECTS IN A THERMOACOUSTIC DEVICE

Kuzuu K.* and Hasegawa S.
*Author for correspondence
Department of Prime Mover Engineering,
Tokai University,
Hiratsuka, Kanagawa 2591292,
Japan,
E-mail: kuzuu@tokai-u.jp

ABSTRACT

A thermoacoustic device, which is operated using thermoacoustic phenomena, has attracted a great deal of attention as an application of renewable heat energy. For a practical application of such device, the correct estimation of thermoacoustic properties is quite important. In the present study, a numerical simulation for thermoacoustic device is performed using computational fluid dynamics (CFD), and the thermodynamic properties are investigated. The results include the temperature flow field and heat flux on the wall. The actual thermoacoustic phenomena are accompanied with nonlinear effects. In order to estimate those effects, the numerical linear analysis is also carried out. Through the comparison of the results of CFD and linear analysis, the linear and nonlinear characteristics of heat transfer in the thermoacoustic device are discussed.

INTRODUCTION

A thermoacoustic device works based on thermoacoustic phenomena, and has the advantage of the inherent thermal efficiency properties of the Stirling cycle and the ability to work using a minimum number of moving parts. From this point of view, a thermoacoustic device is expected as one of applications of renewable heat energy. In fact, since Swift et al. demonstrated the feasibility of this device using an inexpensive prototype [1], many studies of this device and thermoacoustic phenomena have been performed so far.

In such studies, the estimation of thermoacoustic properties plays a key role in determining the design and development for such thermoacoustic device. The linear theory suggested by Rott [2,3] is well known and very useful for the design of thermoacoustic device. However, his theory alone cannot explain the problem of heat transfer in thermoacoustic phenomena. Therefore, in the development of the device, the heat transfer is the important issue to be solved.

NOMENCLATURE

ρ	[kg/m^3]	Density
u	[m/s]	Flow velocity
$\langle u \rangle$	[m/s]	Velocity amplitude
p	[Pa]	Absolute pressure
$\langle p \rangle$	[Pa]	Pressure amplitude
φ	[-]	Phase of acoustic wave
T	[K]	Absolute temperature
n_i	[-]	Normal vector of surface element
t	[s]	Time
Δt	[s]	Period of acoustic wave
f	[Hz]	Frequency of acoustic wave
$\mathcal{V}$	[-]	Volume element of control volume
S	[-]	Surface element of control volume
A	[m^2]	Area of cross section
Br	[-]	Blockage ratio of engine unit
R	[J/kg K]	Gas constant
τ	[Pa]	Viscous stress tensor
q	[W/m^2]	Heat flux vector
μ	[Pa s]	Viscosity
ν	[m^2/s]	Kinematic viscosity
λ	[W/m K]	Thermal conductivity
α	[m^2/s]	Thermal diffusivity
γ	[-]	Specific heat ratio
Pr	[-]	Prandtl number
δ_{ij}	[-]	Kronecker delta
j	[-]	Imaginary unit
ω	[-]	Angular frequency
χ_ν, χ_α	[-]	Thermoacoustic function for viscous and thermal diffusive term
I	[W]	Work flow
W_ν, W_p	[W/m]	Kinetic and potential energy dissipation
W_{prog}	[W/m]	Travelling wave components of work source
W_{stand}	[W/m]	Standing wave components of work source
e	[J]	Internal energy
ϕ	[Pa/s]	Viscous dissipation function
C_p	[J/kg K]	Specific heat at constant pressure

Subscripts

m	Mean (time averaged) value
i	Vector component
ij	Tensor component
pu	Difference between pressure and velocity
r	Cross section value
Hw, Cw	Wall values of hot and cold heat exchangers

Many studies on heat transfer in a thermoacoustic device have been performed recently. Piccolo et al. introduced a simple energy conservation model coupled with classical linear thermoacoustic theory and carried out the numerical analysis [4,5]. They applied their method for the estimation of the heat transfer properties of thermoacoustic heat exchangers. Those

heat exchangers consisted of several parallel plates. Jong et al. also proposed a heat transfer model for one-dimensional oscillatory flow that can be applied to parallel-plate thermoacoustic heat exchangers, and used the model to investigate the heat transfer properties of these heat exchangers [6].

In addition to the above-mentioned linear approach, the numerical simulations by CFD have been also performed so far. This approach is advantageous because the heat transfer properties in a thermoacoustic device can be obtained directly from the calculation results. With respect to such numerical approach, Cao et al. investigated the energy flux density in a thermoacoustic couple under acoustic standing wave conditions [7]. In their study, they estimated the effects of the displacement amplitude on heat transfer. This study is important for heat transfer estimation because the classical Rott's theory [2,3] assumes that the displacement amplitude is negligible compared with the length of the device. In addition, Ishikawa et al. investigated the flow fields and energy transport near the thermoacoustic couples via numerical simulations using a 2D full Navier–Stokes solver [8]. Furthermore, Marx et al. carried out numerical simulations of a thermoacoustic refrigerator that consisted of a resonator and a parallel plate stack [9]. They compared their results with those of linear analysis, and also showed that there is a difference in the mean temperature between the fluid and the plate.

As described above, through many numerical studies, the heat transfer properties in the thermoacoustic device have been investigated. However, it seems that the nonlinear effects in the heat transfer of thermoacoustic device should be discussed more in detail.

In this study, for further discussions of heat transfer, thermodynamic properties are investigated from both CFD and linear analysis, and those results are compared. For CFD, a self-sustained oscillatory flow is reproduced in a standing wave type of thermoacoustic device. In this simulation, a full-scale model of the device was set up. This means that the device includes both the engine unit and full-length resonance tube. The engine unit consists of two heat exchangers and the regenerator. In the linear analysis, the conditions are set up so as to match the thermoacoustic environment in CFD simulation.

NUMERICAL METHOD

A. Calculation method in CFD

The CFD simulations are carried out using the unstructured compressible flow solver LS-FLOW that was developed by the Japan Aerospace eXploration Agency (JAXA) [10]. This solver is based on three-dimensional unsteady compressible Navier–Stokes equations. The solution is based on the finite volume method, and the basic equations are as follows.

$$\frac{\partial}{\partial t}\iiint_V Q\, d\mathcal{V} + \oiint_S (F_e - F_v)\, dS = 0 \qquad (1-1)$$

$$Q = \begin{bmatrix} \rho \\ \rho u_x \\ \rho u_y \\ \rho u_z \\ E \end{bmatrix}, \quad F_e = \begin{bmatrix} \rho U \\ \rho u_x U + n_x p \\ \rho u_y U + n_y p \\ \rho u_z U + n_z p \\ (E+p)U \end{bmatrix}, \quad F_v = \begin{bmatrix} 0 \\ \tau_{xx}n_x + \tau_{yx}n_x + \tau_{zx}n_x \\ \tau_{xy}n_y + \tau_{yy}n_y + \tau_{zy}n_y \\ \tau_{xz}n_z + \tau_{yz}n_z + \tau_{zz}n_z \\ (u_i\tau_{ij} - q_j)n_j \end{bmatrix} \qquad (1-2)$$

$$U = u_x n_x + u_y n_y + u_z n_z\,, \qquad u_i = \begin{bmatrix} u_x \\ u_y \\ u_z \end{bmatrix} \qquad (1-3)$$

$$\tau_{ij} = -\frac{2}{3}\mu(\nabla \cdot U)\delta_{ij} + \mu\left(\frac{\partial u_i}{\partial x_j} + \frac{\partial u_j}{\partial x_i}\right) \qquad (1-4)$$

$$E = \frac{1}{\gamma - 1}p + \frac{1}{2}\rho U^2\,, \qquad q_i = -\lambda\,\nabla T \qquad (1-5)$$

where ρ, u_i, p, T, μ and λ are the density, the velocity vector, the pressure, the temperature, the viscosity and the heat conductivity of the gas, respectively, and n_i is the normal vector to the surface of volume element. The thermodynamic quantities obey the equation of state for a perfect gas, where $p = \rho RT$.

B. Calculation model and conditions for CFD

Figure 1 shows the calculation model used for this simulation. The thermoacoustic device is composed of two resonance tubes and one engine unit. The engine unit has three components: hot and cold heat exchangers (HEX and CEX), and a regenerator (REG). Each component has six flat plates and seven channels, and the components are assembled as shown in the figure. The computational domain is a combination of this device and the buffer region. The calculation model is two-dimensional.

The boundary conditions are also shown in Fig.1. For the velocity on the wall, non-slip condition is given, and for the open end, zero order extrapolation is employed. The wall temperatures, excluding those of the six flat plates of the engine unit, are all fixed at room temperature (298.15 K). The temperatures of the engine unit components are 423.15 K for HEX and 298.15 K for CEX. For the temperature of the REG, a linear distribution ranging between 423.15 K and 298.15 K is used. The working gas is air, the working pressure is $p = 1.01325\times10^5$ Pa, and the temperature $T = 298.15$ K.

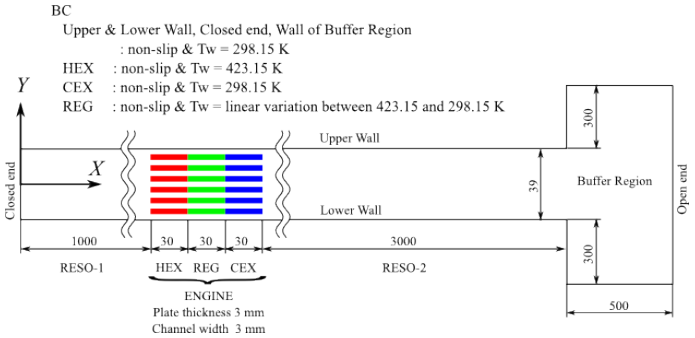

Figure 1 Computational domain and boundary conditions in CFD simulation

In this simulation, the pressure disturbance was subsequently injected as a trigger pulse into the buffer region. The procedure of trigger injection during the simulation is as follows. First, the simulation starts from a static initial condition.

With respect to the initial condition, the air is stationary in whole computational domain. The temperature of the air in RESO-1 and RESO-2 is 298.15 K , and that in the engine unit is given so as to be the same as the wall temperature. This simulation continues without any injection for a while. Then one half cycle of a sinusoidal acoustic wave is injected as a disturbance of $\hat{p} \approx 283$ Pa, which corresponds to the pressure amplitude of 130dB, and $f = 21.2$ Hz from the open end of the buffer region. After that, the supply of this acoustic wave is terminated. A zero-order extrapolation is then used to calculate the boundary variables of the open end, except for the time period when the disturbance is supplied. For convergence criteria, the maximum residual norm of density is set to be less than 1.0×10^{-6}.

C. Calculation model based on linear theory

Extending Rott's linear theory, Piccolo et al. performed numerical estimation for heat transfer of thermoacoustic heat exchanger [4,5]. In their study, this numerical method is employed to calculate temperature field. This is based on the general energy conservation law. Basic equation is as follows.

$$\frac{\partial}{\partial t}\left(\frac{1}{2}\rho U^2 + \rho e\right) = -\nabla \cdot \dot{\mathcal{E}}_i \tag{2}$$

$$\dot{\mathcal{E}}_i = \rho u_i \left(\frac{1}{2}U^2 + h\right) - \lambda \nabla T \tag{3}$$

where $\dot{\mathcal{E}}_i$ and h are the energy flux density vector and the specific enthalpy respectively. In particular, from the assumption of periodic steady state in an acoustic oscillation, the above equation can be transferred to the following time averaged equation.

$$\nabla \cdot \bar{\dot{\mathcal{E}}}_i = 0 \tag{4}$$

$$\bar{\dot{\mathcal{E}}}_i = \frac{\omega}{2\pi}\int_0^{2\pi/\omega} \dot{\mathcal{E}}_i \, dt \tag{5}$$

In the present analysis, the above equation is solved in two-dimensional space. Particularly, both convective enthalpy flux density in the y direction and viscous term are ignored as the first order approximation. The enthalpy flux density in x direction is described as follows.

$$\overline{\dot{h}_x} = \overline{\rho u_x h} = \frac{1}{2Br} Im\left[\frac{(1-\tilde{f}_v)(1-f_\alpha)}{(1-\tilde{\chi}_v)}\right]\langle p\rangle\langle u\rangle$$

$$- \frac{C_p \rho_m}{2\omega\, Br^2(1-Pr)\left|1 - \chi_v\right|^2}$$

$$\times \frac{\partial T_m}{\partial x} Im\left[(1-\tilde{f}_v)(1-f_\alpha)\right]\langle u\rangle^2 \tag{6-1}$$

$$f_v = \frac{\cosh\left((1+j)\,y/\delta_v\right)}{\cosh\left((1+j)\,y_0/\delta_v\right)}, \quad f_\alpha = \frac{\cosh\left((1+j)\,y/\delta_\alpha\right)}{\cosh\left((1+j)\,y_0/\delta_\alpha\right)} \tag{6-2}$$

$$\chi_v = \frac{\tanh\left((1+j)\,y_0/\delta_v\right)}{(1+j)\,y_0/\delta_v}, \quad \chi_\alpha = \frac{\tanh\left((1+j)\,y_0/\delta_\alpha\right)}{(1+j)\,y_0/\delta_\alpha} \tag{6-3}$$

$$\delta_v = \sqrt{2\nu/\omega}, \quad \delta_\alpha = \sqrt{2\alpha/\omega} \tag{6-4}$$

On the other hand, from the first order approximation, the amplitudes of temperature and flow velocity are as follows.

$$\langle T\rangle = \frac{1}{\rho_m C_p}(1-f_\alpha)\langle p\rangle$$

$$- \frac{1}{\rho_m \omega^2(1-Pr)}\frac{d\langle p\rangle}{dx}\frac{\partial T_m}{\partial x}\left[(1-f_\alpha) - Pr(1-f_v)\right] \tag{7}$$

$$\langle u\rangle = \frac{j}{\omega\rho_m}\frac{d\langle p\rangle}{dx}(1-f_v) \tag{8}$$

Here, y_0 is one half of the two-dimensional channel width.

Calculation conditions are setup so as to match CFD simulation shown in Fig.1. However, the computational domain is limited to the central channel of the engine unit. For the pressure amplitude at a pressure antinode, which is required for this analysis, the CFD result is employed, and the pressure amplitude at the central position of the engine unit is calculated from sinusoidal curve of standing wave generated in the device. Furthermore, the symmetrical condition is applied to the center plane in the y direction. The computational domain and geometry are shown in Fig.2.

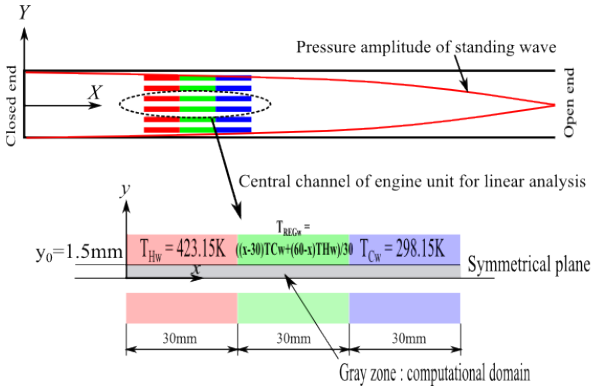

Figure 2 Computational domain and boundary conditions in linear analysis

RESULTS AND DISCUSSION

A. Velocity field behavior

First, velocity field behavior of the self-sustained oscillatory flow in CFD is shown in Fig.3. This graph shows time variation of the axial velocity at $(x, y) = (1.04, 0.0)$. The injection time of the acoustic signal is $t = 2.054\ to\ 2.078$ seconds. As shown in the figure, the phenomenon is considered to be in the periodic steady state after 4 seconds.

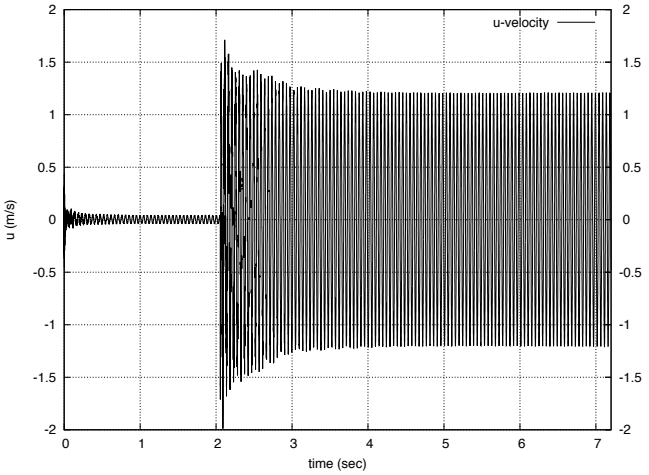

Figure 3 Time variation of axial velocity in the engine unit (CFD result)

B. Time averaged temperature field

From the CFD results, time averaged temperature field around the engine unit is visualized. Figure 4 shows two-dimensional distribution of averaged temperature. Since the temperature of top and bottom wall is given as the room temperature (T_w=298.15K), the distribution in top and bottom channels is not symmetrical for the central plane of each channel. On the other hand, with respect to the results in the other channels, temperature field shows almost the same behaviour, and both distributions are symmetrical. This implies that the flow behaviour within top and bottom channels does not affect the flow of the inside channels. Another feature is the fact that there is thermal buffer region in the outer side of HEX. This is typical behaviour observed in the heat exchanger of thermoacoustic device. This phenomenon generates the leak of the engine unit.

Next, in order to investigate the linear or nonlinear characteristics of temperature field behaviour, the CFD result is compared with that of the linear analysis. As shown in Fig.5, there is a good agreement in both of results. It is possible that the strong non-linear phenomena do not appear in the central region of the engine unit. Figure 6 shows the temperature distribution on each section in the y direction. This graph also shows quantitative agreement between CFD and linear analysis. However, with respect to the temperature near the exit/entrance of HEX (x=0), the small difference is observed. This might be due to the thermal buffer region, which is not considered in the linear analysis.

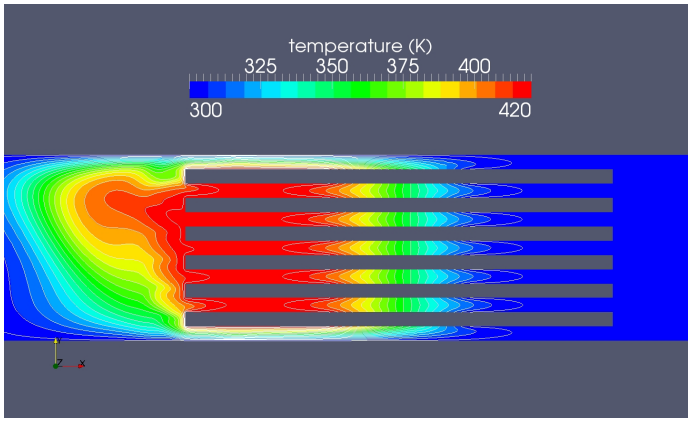

Figure 4 Time averaged temperature field around the engine unit (CFD result)

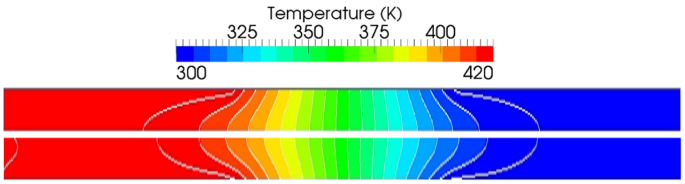

Figure 5 Comparison of time averaged temperature distribution in the central channel between linear analysis (upper) and CFD (lower)

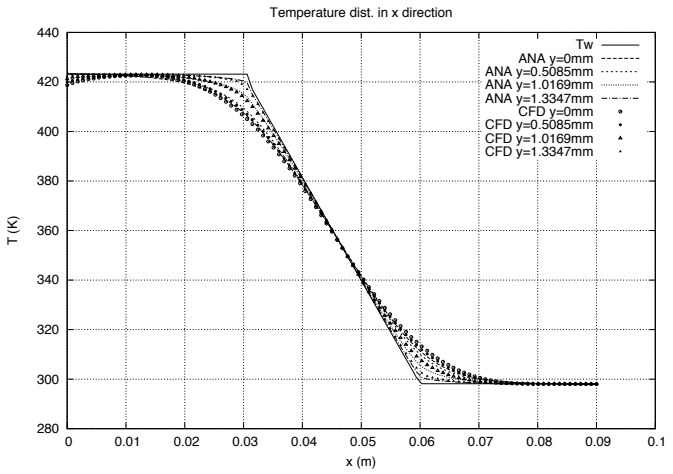

Figure 6 Comparison of time averaged temperature in the central channel in the x direction

C. Inflow and outflow of heat on the wall

Next, the heat flux on the wall is investigated from the results of CFD and linear analysis. Figure 7 shows the comparison of those results. Here, the positive value describes the flux toward fluid region. There is a good agreement except near exit/entrance area of HEX (x=0 to 0.01m). It is clear that this difference is due to the existence of thermal buffer

observed in CFD. Actually, in CFD result, the heat energy leaks toward outside and temperature decreases slightly in this region. This is shown in Fig.6. On the other hand, the agreement in other region implies that the behaviour of heat flow keeps linearity as well as the fluid flow. Furthermore, this agreement shows a significant knowledge for heat flow in thermoacoustic phenomena. In this simulation, while the heat flux is calculated from the time integration of instantaneous heat flux in CFD, the heat flux calculation in linear analysis is based on time averaged temperature distribution. As shown in the previous section, time averaged temperature distribution has already shown the agreement between CFD and linear analysis. Furthermore, Figs 8 (a)-(b) show that there is also a good agreement for the distribution within the section in the x direction. These facts implies that time averaged value of instantaneous heat flux agrees with the heat flux based on the gradient of time averaged temperature as shown in Eqn. (9).

$$\overline{q_{wall}} = \frac{\omega}{2\pi}\int_0^{2\pi/\omega} \lambda\left(\frac{\partial T(y,t)}{\partial y}\right)_{y=y_0} dt$$

$$\cong \lambda\left(\frac{\partial \overline{T(y)}}{\partial y}\right)_{y=y_0} \quad (9)$$

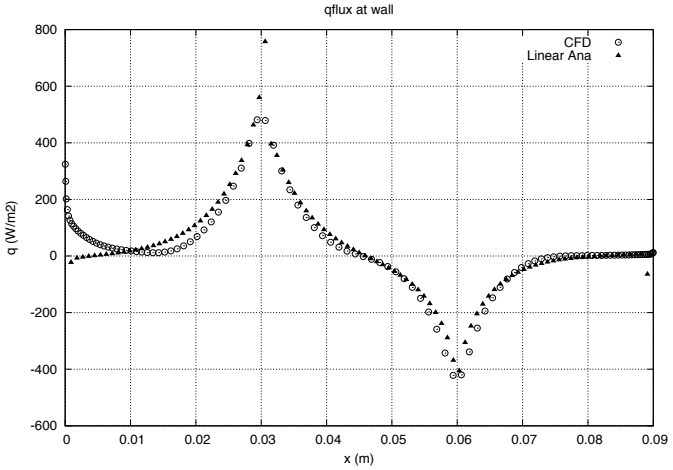

Figure 7 Comparison of heat flux on the wall between CFD and linear analysis. (positive : inflow flux into the fluid)

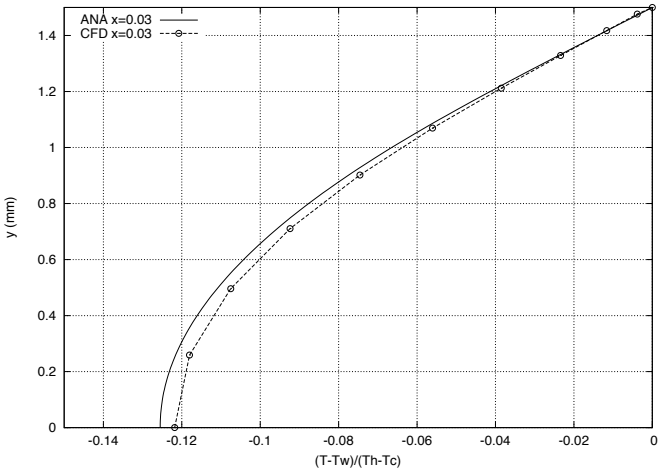

(a) maximum heat flux section (x=0.03m)

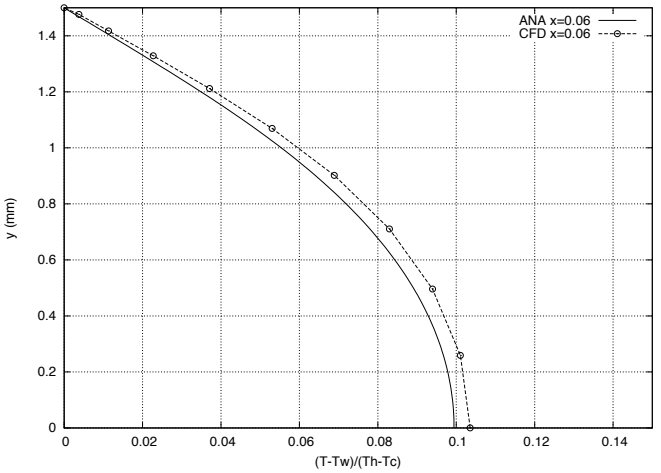

(b) minimum heat flux section (x=0.06m)

Figure 8 Temperature distribution within the cross section

Finally, the behaviour of temperature amplitude is discussed. In CFD simulation, temperature oscillation becomes asymmetry in the x direction at the section where the heat exchanger changes to the regenerator (x=0.03 and 0.06m). This is due to the non-uniformity of temperature gradient in the x direction. Figures 9 (a)-(b) show the temperature amplitude at each section (x=0.03 and 0.06m). The lines (described by CFD ampl1 and ampl2) in these graphs show the asymmetrical feature. On the other hand, temperature amplitude calculated from linear analysis (Eqn. (7)) is shown by symbols (ANA_ampl1_loc and ANA_ampl2_loc). Those distributions are symmetrical and do not agree with CFD results. However, when superposed with time averaged temperature (ANA ampl1 and ampl2), the amplitude distributions agree with CFD results. This fact is consistent with the discussion for time averaged heat flux on the wall.

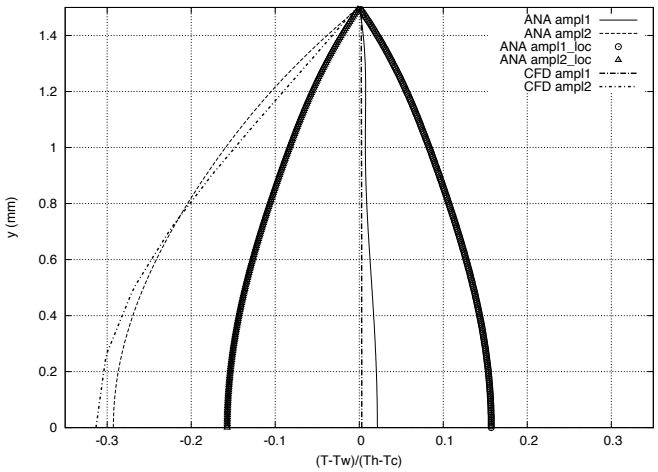

(a) maximum heat flux section (x=0.03m)

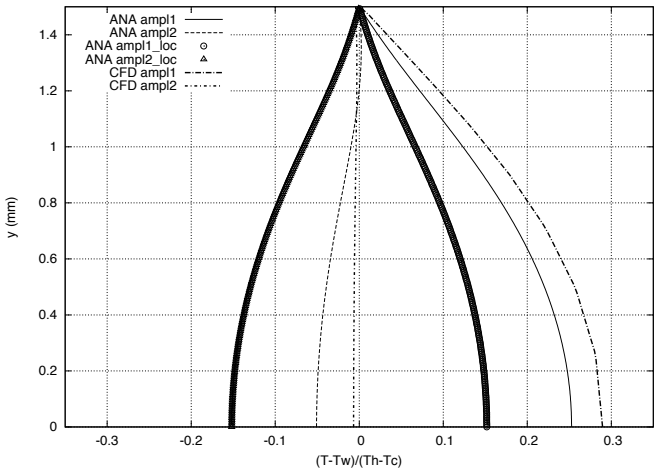

(b) minimum heat flux section (x=0.06m)

Figure 9 Temperature amplitude within the cross section

SUMMARY

Through numerical simulation by CFD and linear analysis, heat transfer in a thermoacoustic device was discussed. From the comparison of both results, even though the employed linear analysis is due to the fist order approximation, it is applicable to large area of the actual engine unit. However, there are slight differences near the exit/entrance area of the hot heat exchanger. It is possible that this fact affects the net heat flow. This implies that the effect of thermal buffer region should be considered in the linear analysis.

ACKNOWLEDGMENTS

This work was supported by the Japan Science and Technology Agency through the Advanced Low Carbon Technology Research and Development Program.

REFERENCES

[1] S. N. Backhaus and G. W. Swift, "A thermoacoustic Stirling heat engine," Nature 399, 1999, pp. 335–338

[2] N. Rott, "Damped and thermally driven acoustic oscillations in wide and narrow tubes," *Z. Angew. Math. Phys.*, 20(2), 1969, pp. 230–243

[3] N. Rott, "Thermally driven acoustic oscillations, part III: Second-order heat áux," *Z. Angew. Math. Phys.*, 26, 1975, pp. 43-49

[4] A. Piccolo and G. Pistone, "Estimation of heat transfer coefficients in oscillating flows: The thermoacoustic case," *International Journal of Heat and Mass Transfer,* 49, 2006, pp.1631-1642

[5] A. Piccolo, "Numerical computation for parallel plate thermoacoustic heat exchangers in standing wave oscillatory flow," *International Journal of Heat and Mass Transfer,* 54, 2011, pp. 4518-4530

[6] J. A. de Jong, Y. H. Wijnant, and A. de Boer, "A one-dimensional heat transfer model for parallel-plate thermoacoustic heat exchangers," *J. Acoust. Soc. Am.*, 135(3), 2014

[7] N. Cao, J. R. Olson, G. W. Swift, and S. Chen, "Energy flux density in a thermoacoustic couple," *J. Acoust. Soc. Am.*, 99(6), 1996

[8] H. Ishikawa and D. J. Mee, "Numerical investings of flow and energy fields near a thermoacoustic couple," *J. Acoust. Soc. Am.*, **111**(2), 2002

[9] D. Marx and Ph. Blanc-Benon, "Numerical calculation of the tempature difference between the extremities of a thermoacoustic stack plate," *Cryogenics*, **45**, 2005, pp. 163-172

[10] K. Fujimoto and K. Fujii, "Study on the Automated CFD Analysis tools for Conceptual Design of Space Transportation Vehicle," *FEDSM 2007-37128, Proc. 5th ASME/JSME Jount Fluid Engineering Conference,* 2007